ADVANCES IN MATERIALS SCIENCE, Vol. 26, No. 1 (87), March 2026

DOI: 10.2478/adms-2026-0004

Ting-Hsueh Chuang[1], Fwu-Hsing Liu[1], Chung-Chen Tsao[1], Chin-Guo Kuo[2]*, Chun-Yao Hsu[1]*

[1]*Department of Mechanical Engineering, Lunghwa University of Science and Technology, Taoyuan 33306, Taiwan*
[2]*Department of Industrial Education, National Taiwan Normal University, Taipei 10610, Taiwan*

** t07019@ntnu.edu.tw (C.G. Kuo), cyhsu@mail.lhu.edu.tw (C.Y. Hsu)*

OPTIMIZATION OF MECHANICAL PROPERTIES AND FEATURES OF ELECTROLESS Ni-P-Zr TERNARY PLATING USING THE GREY-TAGUCHI METHOD

ABSTRACT

Electroless Ni-P-Zr films are deposited onto Al substrates. Effect of different pre-treatments on the subsequent chemical plating. XRD analysis shows that the Ni-P-Zr film is amorphous. Grey-Taguchi shows that the Ni-P-Zr coating exhibits a friction coefficient of 0.35, a corrosion potential of –0.60 V, a Vickers hardness of 582.9 HV, and a fatigue life of 52 times. A comparison of fatigue failure mechanisms for the uncoated substrate and the electroless Ni-P-Zr coating is conducted under high-strain low-cycle fatigue loading. The results confirm that the coating eliminates crack initiation and propagation and increases the fatigue life of the specimens.

Keywords*: Electroless Ni-P-Zr, mechanical properties, fatigue*

INTRODUCTION

Electroless nickel plating is an autocatalytic deposition process that renders exceptional physical, electrical, tribological, mechanical, and corrosion-resistant properties [1]. This hard coating is widely used in chemistry, machinery, automobiles, electronics, aerospace engineering and the food industry. Electroless plating adheres well to metal and non-metal products and its thickness is almost uniform, even for parts with complex shapes [2]. The electroless plating bath is composed of an aqueous solution that contains nickel ions as the metal source, a stabilizer to prevent premature decomposition of the solution, a reducing agent to provide electrons and a complexing agent to maintain the chemical stability of the plating solution [3]. These systems function within a specific range of temperature, pH and metal ion concentrations.

Aluminum and its alloys are widely used in many industrial fields due to their high specific strength and good machinability. However, aluminum alloys feature low hardness and poor wear resistance so they cannot be used for some engineering applications. Previous

Received: 21.11.2025; Received in revised form: 26.01.2026; Accepted: 3.02.2026

studies show that these features are improved by electroless plating of a surface protective layer [4]. Arumugam et al. [5] studied electroless plating on an Al alloy substrate and produced a Ni-P coating with uniform thickness, wear resistance, corrosion resistance and high hardness. The result shows that the surfactant (sodium lauryl sulfate) and passive additive (Al_2O_3) significantly improve the surface finish, microhardness, microstructure and wear rate for Ni-P coatings. Qin [6] studied the electroless plating of Ni-P alloy on the surface of a 6061 Al alloy substrate using sodium hypophosphite as a reducing agent. The results show that the Ni-P coating film is amorphous and significantly increases the aluminum alloy's resistance to corrosion.

A conventional experimental method often requires a significant number of trials to evaluate multiple parameters, which is time-consuming and costly. The Taguchi approach uses principles of experimental design with a quality loss function and orthogonal arrays to significantly reduce the number of experimental runs. The Taguchi methodology increases experimental efficiency and enables the development of high-quality, low-cost products [7]. It is widely used in many engineering fields to optimize fabrication processes and to increase product performance. There are many studies of electroless plating but the use of the Taguchi method to create optimal process parameters for the coating has industrial applications and academic value.

The grey-Taguchi method is a practical approach that combines experimental design with statistical analysis to increase product quality. This method considers multiple quality characteristics simultaneously and is a cost-effective solution for optimizing complex processes for a wide range of applications. Agrawal et al. [8] produced electroless Ni-B-W coatings using the grey-Taguchi method to determine multi-objective optimized deposition parameters and improve the mechanical properties and thermal stability of the coating film. By optimizing the combination of multi-objective parameters using grey-Taguchi analysis, electroless plating Ni-P-SiC nanocomposite coatings have a lower coefficient of friction so wear resistance is increased [9].

Gultekin et al. [10] demonstrated that electroless coating of the ternary Ni-P-W alloy imbues better tribological and anti-corrosive performance than its binary counterpart. Biswas et al. [11] showed that electroless Ni-P-Cu ternary alloy exhibits high hardness, excellent corrosion resistance and strong wear resistance. Ternary alloys electroless plating has many superior properties, as demonstrated by numerous studies [12]. Zr alloys are commonly used as cladding and structural materials in nuclear reactors due to their superior neutron economy, strong mechanical properties and high resistance to corrosion [13]. An alkaline electroless plating solution that uses an in-situ co-precipitation reaction has been used for the deposition of Ni-P-ZrO_2/Al_2O_3/Al_3Zr composite coatings on various substrates, including commercial aluminum, low-carbon steel and carbon fiber cloth [14]. Few studies use electroless Ni-P-Zr plating but the thin film of this plating has excellent mechanical properties and corrosion resistance so it warrants further research. This study employs multiple performance characteristics combined with grey-Taguchi analysis, following a similar methodology to that used by Zhao et al. [15]. While Zhao et al. investigated a ZrWN/buffer layer multilayer film deposited via direct current reactive magnetron sputtering, our research focuses on optimizing the electroless plating process for depositing a Ni-P-Zr ternary alloy film onto an Al 6061-T6 substrate.

Ganesan et al. [16] reported that Al alloy is widely used in the automotive and aerospace industries. These parts are subjected to cyclic loads during operation and are prone to fatigue failure, but the fatigue strength of aluminum alloys is lower than that of steel, so increasing

the fatigue performance of aluminum alloys reduces failure repairs and related costs. Electroless plating surface modification increases the fatigue performance of parts [17]. This study determines the failure mechanism under high-strain and low-cycle fatigue loads in an Al substrate that features electroless Ni-P-Zr plating. The elemental composition, microstructure, microhardness and corrosion resistance of the coating are determined.

EXPERIMENTAL PROCEDURE

The chemical composition and mechanical properties of the Al 6061-T6 sample (plate 45 × 10 × 4 mm³) are detailed in Reference [18]. The surface of the Al substrate was polished using #300, #600, and #800 sandpaper in sequence and the test piece was cleaned with alcohol. Before electroless plating, the Al substrate was subject to pretreatments, including roughening and activation, to render the surface catalytically active [19]. The electroless plating bath composition included: Zr $(SO_4)_2$ (20 g/L) +$NiSO_4$ (30 g/L) + $Na_3C_6H_5O_7 \cdot 2H_2O$ (45 g/L) + NH_4Cl (35 g/L) + $NaPH_2O_2 \cdot H_2O$ (30 g/L). A Taguchi experimental design and L_9 (3^4) orthogonal array were used to establish the electroless plating parameter levels, including solution pH value (6, 8, 10), bath temperature (60, 70, 80°C), deposition time (15, 30, 60 min) and stirring rate (0, 150, 300 rpm). Table 1 shows the Al substrate pretreatment and electroless Ni-P-Zr film plating parameters. The Al alloy substrates were pretreated using two different formulations: formula A and formula B (see Table 1). Ni-P-Zr films were then deposited via electroless plating.

Formula A: Remove Al substrate surface organic/oxide layers, phosphate and carbonate act as complexing agents and buffering salts, activate the surface and deposit a thin zinc-based activation layer to increase the adhesion of subsequent electroless coatings. Formula B: Alkaline degreasing and etching removes organic and loosely bonded oxides. The chromic acid–sulfuric acid mixture removes tenacious oxide layers and creates a micro-roughened surface to promote mechanical anchoring. HCl pickling ensures complete oxide and hydroxide removal to produce a reactive surface that allows catalytic initiation of electroless plating [20]. The films' surface morphology, cross-sectional structure and elemental content were measured using field emission scanning electron microscopy and energy-dispersive X-ray spectroscopy (EDS). The structural properties and micro-hardness of the film were measured using an X-ray diffractometer (Rigaku-2000 X-ray Generator) with a grazing incidence angle of 2° and a nano-indenter (ASMEC UNAT). High-resolution transmission electron microscopy (TEM, FEI Tecnai F20) was utilized to determine the microstructure of the coated film. The coefficient of friction (CoF) of the coating film was measured using a ball-on-disk tester (CSM Equipment, Switzerland). The dry test used an Al_2O_3 ceramic ball with a 3.0 mm radius, a total sliding distance of 100 m and a normal load of 2.5 N [21]. The hardness of the films was measured using a nano-indenter (ASME CUNAT).

The corrosion behavior of the film was measured using a potentiostat/galvanostat (EG&G Model 263A) in a 3.5 wt% NaCl solution. The values for corrosion potential (Ecorr, Volt) and corrosion current density (Icorr, Amp/cm^2) were determined from the polarization curves and calculated using the Tafel extrapolation method [22]. A fatigue testing method accelerated fatigue damage under high-strain cycling conditions [23]. Figure 1 shows the 60° bending fatigue testing apparatus (R = –1, reverse stress mode). This high-strain and low-cycle apparatus is specifically designed to promote the early onset of fatigue fracture and to measure the performance of electroless coatings.

Table 1. *Al substrate pretreatment and electroless Ni-P-Zr film plating parameters*

Al 6061-T6 plate 45 × 10 × 1 mm³.
Al substrate pretreatment is done using two different formulas [19].

Formula A:
step 1. [Na_2CO_3 (25 g/L) + Na_3PO_4 (25 g/L), 80°C, immerse for 3 min].
step 2. [$Na_3PO_4 \cdot 12H_2O$ (35 g/L) + Na_2CO_3 (25 g/L) + NaOH (10 g/L), 70 °C, immerse for 2 min].
step 3. [ZnO (5 g/L) + $KNaC_4H_4O_6 \cdot 4H_2O$ (500 g/L) + NaOH (10 g/L) + HNO_3 (500 g/L), room temperature, immerse for 1.5 min].

Formula B:
step 1. [Na_2CO_3 (40 g/L) + Na_3PO_4 (25 g/L) + NaOH(10 g/L), 80°C, immerse for 3 min]. step 2. [H_2CrO_4(80 g/L) + H_2SO_4 (80 g/L), room temperature, immerse for 8 min].
step 3. [HCl (360 g/L), room temperature, immerse for 3 min].

Electroless plating bath composition:
$Zr(SO_4)_2$ (20 g/L) +$NiSO_4$ (30 g/L) + $Na_3C_6H_5O_7 \cdot 2H_2O$ (45 g/L) + NH_4Cl (35 g/L) + $NaH_2PO_2 \cdot H_2O$ (30 g/L)

Symbol	Control factor	Level 1	Level 2	Level 3
A	pH value	6	8	10
B	bath temperature (°C)	60	70	80
C	deposition time (min)	15	30	60
D	stirring rate (rpm)	0	150	300

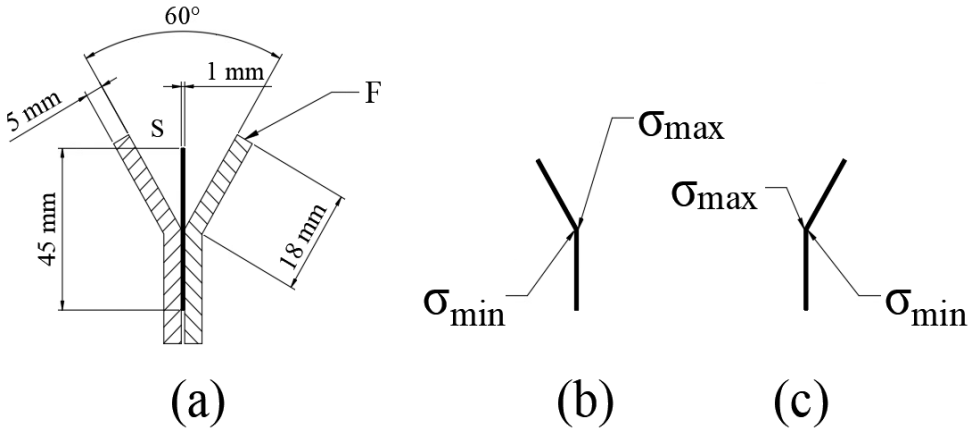

Fig. 1. Schematic diagram of a high-strain, low-cycle bending fatigue (60°) test device, using a complete reversal of fatigue stress cycles (R = –1, reverse stress mode): (a) sample in the neutral position, where **F** indicates the fixture and **S** represents the Al substrate (plate 45 × 10 × 4 mm³), (b) sample bent to the left and (c) sample bent to the right [23]

RESULTS AND DISCUSSION

Al substrate pretreatment and electroless plating

The surface of the substrate was modified and pretreated to increase adhesion between the coating and the substrate and an intact electroless plating film was produced [24]. The aluminum alloy substrates were subjected to two different pretreatment protocols—Formula A and Formula B (summarized in Table 1)—prior to the electroless deposition of Ni-P-Zr films. The plating solution consisted of Zr $(SO_4)_2$ (20 g/L), $NiSO_4$ (30 g/L), $Na_3C_6H_5O_7 \cdot 2H_2O$ (45 g/L), NH_4Cl (35 g/L) and $NaPH_2O_2 \cdot H_2O$ (30 g/L). The deposition was performed at pH 10 and the plating bath was maintained at 80°C for 60 minutes and stirred at a rate of 300 rpm.

Fig. 2a shows the pretreatment for the Al substrate using formula A. The sample surface was roughened and activated to allow the electroless plating process. Fig. 2b shows that subsequent to the electroless plating process, the Ni-P-Zr film completely covers the substrate surface and a good coating film is produced. Fig. 3a shows the pretreatment for the Al substrate using formula B. Fig. 3b shows that the Ni-P-Zr film coating is uneven, the coverage is incomplete and the coating film is poor. Excessive roughening and activation pretreatment create large micropores on the substrate's surface, which is not conducive to the subsequent electroless process. Similar to the results of the study by Mandal et al. [20], the results of this study show that surface roughness (roughness below 338 nm) must not be excessive to obtain good coating films. Formulation B also lacks a zinc-based activation layer, which is detrimental to subsequent electroless thin film deposition. During electroless plating, Zn is displaced by Ni and autocatalytic Ni-P growth then promotes a uniform coating [25].

Table 2 lists the Ni-P-Zr films' hardness, fatigue test results and friction coefficient for different substrate pretreatments (Formula A and Formula B). For bare Al 6061-T6 substrates without coating, the hardness is 392.9 HV, the fatigue life is 30 times and the friction coefficient is 0.66. The Ni-P-Zr ternary film coating performs better than the uncoated Al substrate. Using Formula A, the Al surface is roughened and activated. Subsequent electroless film plating was used to obtain a high-quality Ni-P-Zr film. The Ni-P-Zr film is respectively better in terms of hardness, fatigue life and friction coefficient by 35.17%, 36.67%, and 34.84%. Tafel analysis of the potentiodynamic polarization curves shows the corrosion behavior of the coating samples. Fig. 4 shows the polarization curves for Ni-P-Zr films using different substrate pretreatments. The corrosion potential is calculated for bare Al (-1.18 V) and Ni-P-Zr film-coated samples using formula A (-0.67 V) and formula B (-1.01 V).

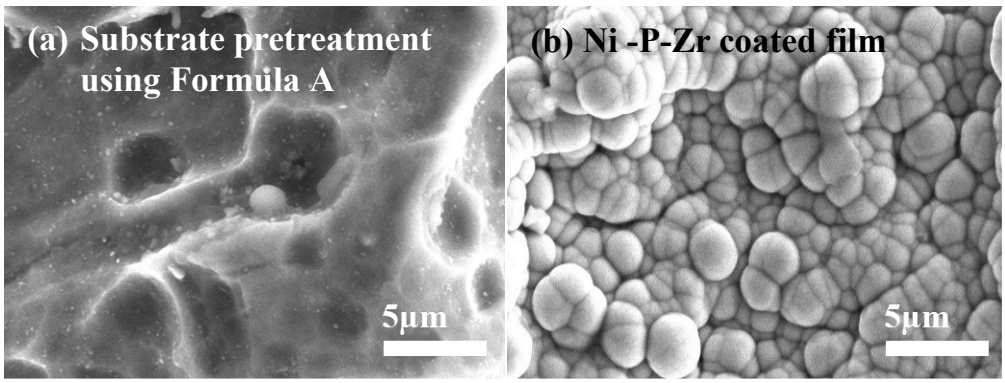

Fig. 2. SEM images for substrate pretreatment and Ni-P-Zr coated film, using Formula A

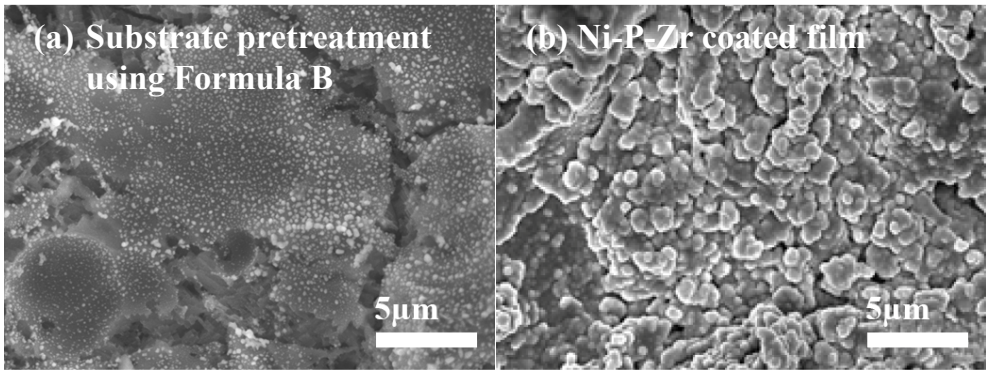

Fig. 3. SEM images for substrate pretreatment and Ni-P-Zr coated film, using Formula B

Table 2. *Hardness, fatigue test results and friction coefficient for Ni-P-Zr films that use different substrate pretreatments*

	Test 1	Test 2	Avg.	Improvement rate (%)
	Vickers-Hardness (HV)			
Al original	391.9	393.9	392.9	
Formula A	525.1	537.2	531.1	35.17
Formula B	406.3	411.8	409.1	4.12
	Fatigue test (no. of bends)			
Al original	29	31	30	
Formula A	40	42	41	36.67
Formula B	32	30	31	3.33
	Friction coefficient (CoF)			
Al original	0.67	0.65	0.66	
Formula A	0.41	0.44	0.43	34.84
Formula B	0.61	0.65	0.63	4.24

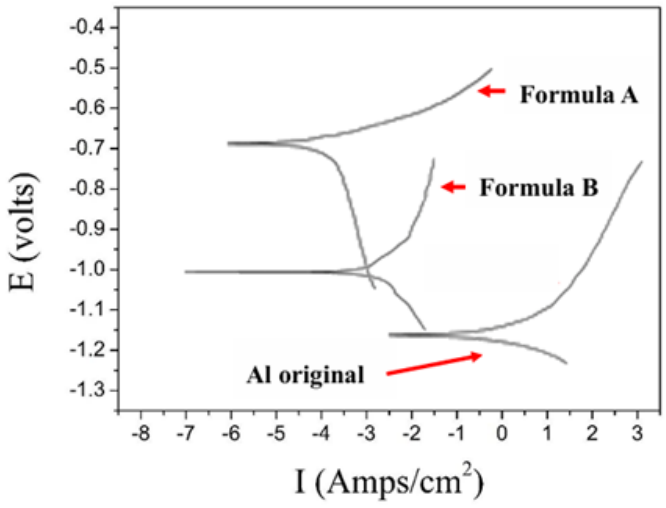

Fig. 4. Polarization curves for uncoated Al and coated Ni-P-Zr films in aqueous solution

Electroless plating using grey-Taguchi analysis

Using Taguchi quality engineering principles, this study established the control factors and their corresponding experimental levels, as shown in Table 1. Fig. 5 (a) shows the X-ray diffraction patterns for electroless N-P-Zr composite film. The pattern features one broadened peak at 2θ = 42.4 °, which shows that the films are amorphous [26, 27]. Fig. 5 (b) shows a high-resolution TEM image, where the lack of a clearly defined long-range ordered structure confirms that the nanoparticles exhibit an amorphous phase. Fig. 5 (c) displays the selected area electron diffraction (SAED) pattern of the Ni-P-Zr film, characterized by a diffuse ring pattern, which is a hallmark of an amorphous structure. Table 3 lists the experimental L_9 (3^4) results for the friction coefficient, corrosion potential and Vickers hardness value for Ni-P-Zr films and the signal-to-noise ratio (S/N). The friction coefficient ranges from 0.37 to 0.61, the corrosion potential ranges from -0.66 to -0.60 V and the Vickers hardness ranges from 459.4 to 541.5 HV. When Ni-P-Zr film is plated, the Vickers hardness and corrosion potential increase and the friction coefficient decreases. All coated samples feature better mechanical properties than the uncoated Al samples. Table 4 shows results for the ANOVA for the coefficient of friction, the corrosion potential and the Vickers hardness. The pH value has the most significant effect on the friction coefficient (P=75.69%) and the Vickers hardness (P=77.45%). The bath temperature has the most significant effect on corrosion potential, with P = 34.24% contribution.

Table 3. *Experimental L_9 (3^4) results for the friction coefficient, corrosion potential, and Vickers hardness value for Ni-P-Zr films and signal-to-noise (S/N) ratio*

No.	Factors				Friction coefficient			S/N (dB)	Corrosion potential (Volts)			S/N (dB)	Hardness (HV)			S/N (dB)
	A	B	C	D	F_1	F_2	Ave.		C_1	C_2	Ave.		H_1	H_2	Ave.	
1	1	1	1	1	0.60	0.59	0.60	4.51	-0.62	-0.61	-0.62	4.22	480.8	509.6	495.2	53.90
2	1	2	2	2	0.61	0.61	0.61	4.29	-0.64	-0.61	-0.63	4.08	451.2	502.6	476.9	53.57
3	1	3	3	3	0.51	0.50	0.51	5.93	-0.61	-0.62	-0.62	4.22	499.6	522.6	511.1	54.17
4	2	1	2	3	0.48	0.49	0.49	6.29	-0.63	-0.66	-0.65	3.81	461.6	465.6	463.6	53.32
5	2	2	3	1	0.44	0.43	0.44	7.23	-0.65	-0.64	-0.65	3.81	462.6	534.1	498.4	53.95
6	2	3	1	2	0.43	0.45	0.44	7.13	-0.63	-0.64	-0.64	3.94	452.7	466.1	459.4	53.24
7	3	1	3	2	0.46	0.46	0.46	6.71	-0.60	-0.59	-0.60	4.51	567.2	501.5	534.4	54.56
8	3	2	1	3	0.36	0.37	0.37	8.75	-0.65	-0.67	-0.66	3.61	556.6	526.4	541.5	54.67
9	3	3	2	1	0.41	0.40	0.41	7.85	-0.61	-0.61	-0.61	4.29	502.3	556.8	529.6	54.48
Al 6061-T6					0.65	0.67	0.66		-1.04 -1.31		-1.18		391.9	393.9	392.9	

Note: A is pH value, B is bath temperature, C is deposition time and D is stirring rate.

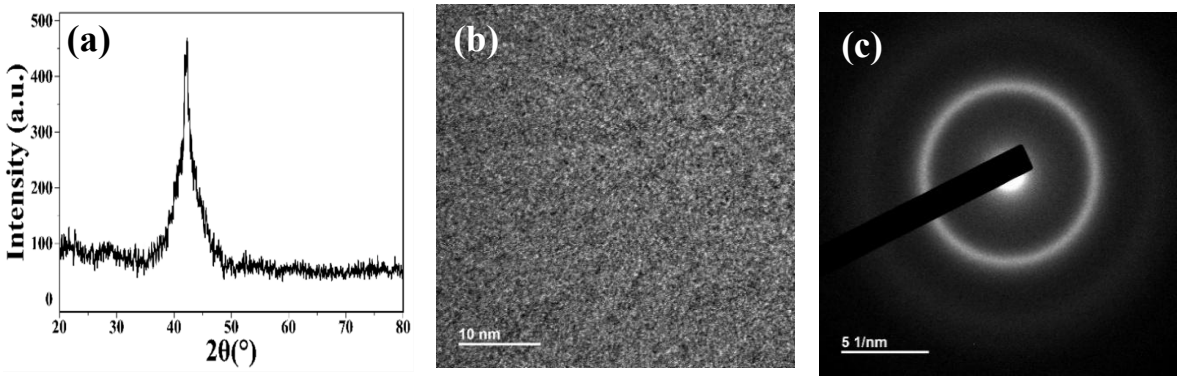

Fig. 5. Electroless N-P-Zr film, (a) X-ray diffraction pattern, (b) high-resolution TEM image, and (c) electronic diffraction pattern

Table 4. *ANOVA results for the coefficient of friction, the corrosion potential, and the Vickers hardness, corresponding to Table 3*

Factor	S/N ratio (dB)			Degree of freedom	Sum of square	Variance	Contribution (P %)
	Level 1	Level 2	Level 3				
Coefficient of friction							
A	4.91	6.88	7.78	2	12.93	6.47	75.69
B	5.85	6.76	6.97	2	2.14	1.07	12.55
C	6.80	6.14	6.64	2	0.70	0.35	4.09
D	6.53	6.06	6.99	2	1.31	0.66	7.67
Total				8	17.07		100.00
Corrosion potential							
A	-4.18	-3.85	-4.14	2	0.19	0.09	28.39
B	-4.18	-3.83	-4.15	2	0.22	0.11	34.24
C	-3.93	-4.06	-4.18	2	0.10	0.05	14.96
D	-4.11	-4.18	-3.88	2	0.15	0.07	22.41
Total				8	0.65		100.00
Vickers hardness							
A	51.91	51.44	52.77	2	2.72	1.36	77.45
B	51.97	52.14	52.02	2	0.05	0.02	1.38
C	51.98	51.80	52.35	2	0.47	0.23	13.27
D	52.20	51.80	52.13	2	0.28	0.14	7.90
Total				8	3.52		100.00

Grey relational analysis is used to interpret complex relationships between multiple variables or performance indicators. It allows comparison and decision-making for systems for which there is limited or uncertain information by measuring the degree of similarity or influence between factors using a grey relational coefficient [28]:

$$r(x_o(k), x_i(k)) = \frac{\min\limits_i \min\limits_k |x_0(k) - x_i(k)| + \zeta \max\limits_i \max\limits_k |x_0(k) - x_i(k)|}{|x_0(k) - x_i(k)| + \zeta \max\limits_i \max\limits_k |x_0(k) - x_i(k)|} \quad (1)$$

where, $x_i(k)$ represents the normalized value of the k^{th} performance characteristic in the i^{th} experiment and ζ denotes the distinguishing coefficient, which typically falls within the range $\zeta \in [0,\ 1]$. This coefficient can be adjusted in terms of the specific requirements of the system. For this study, all electroless plating parameters are considered to have equal importance; so ζ has a value of 0.5.

The average value of the grey relational coefficients is used to represent the grey relational grade. This value serves as an overall measure of the relationship between each experimental trial and the ideal reference and is calculated as [28]:

$$r(x_0, x_i) = \frac{1}{n} \sum_{k=1}^{n} r(r_0(k), x_i(k)) \quad (2)$$

where, n denotes the total number of performance characteristics for the analysis.

To evaluate the multiple response performance characteristics, all experimental data is processed using the grey relational grade. Eqs. (1) and (2) are used to calculate the grey relational grade for each experiment in the L_9 orthogonal array and the results are shown in Table 5. Table 6 shows the ANOVA results for the multiple quality properties of the electroless N-P-Zr composite film coating process. The grey relational analysis shows that the pH value is the most influential factor, contributing 83.31% to the overall performance.

A higher grey relational grade indicates that the product quality is closer to the ideal value so a larger grade is more desirable [28]. For this study, the optimal multiple quality characteristics for the electroless N-P-Zr film coating are achieved using the orthogonal array parameters $A_3B_2C_1D_3$ (Experiment No. 8, Table 5). The grey relational prediction identifies the optimal condition as $A_3B_2C_3D_3$ (see Table 6), which corresponds to a pH of 10, a bath temperature of 70°C, a deposition time of 60 minutes and a stirring rate of 300 rpm.

The verification experiment results for the multiple quality properties of the electroless N-Zr-P film coating are shown in Table 7. The optimized parameters ($A_3B_2C_3D_3$) give better performance than the orthogonal array conditions ($A_3B_2C_1D_3$): the friction coefficient decreases from 0.37 to 0.35, the corrosion potential increases from -0.66 V to -0.60 V and the Vickers hardness increases from 541.5 to 582.9 HV. Table 8 shows the chemical composition of the Ni-P-Zr films, as determined by energy-dispersive spectrometry (EDS). The results show that a composition of approximately 96.02 wt% Ni, 1.37 wt% Zr, and 2.61 wt% P yields favorable multiple quality characteristics for the Ni-P-Zr film coating. This is in agreement with the results of Ghaderi et al [29], who showed that a decrease in phosphorus content increases the hardness of the coatings. The decrease in hardness for electroless coatings with

high phosphorus content is primarily due to the formation of intermetallic phases that are softer than the face-centered cubic crystalline nickel phase. Agarwala et al [30] showed that electroless plating with low phosphorus content (2% to 3 wt.%) exhibits greater hardness than plating with high phosphorus content (10% to 12 wt.%). In its as-deposited state, the Ni-P-Zr electroless coating maintains an amorphous structure, so phosphorus atoms are randomly distributed between the nickel atoms within the matrix [31].

For comparison, the electroless ternary Ni-P-W plating solution replaces $Zr(SO_4)_2$ with $Na_2WO_4{\cdot}2H_2O$ and the remaining chemical baths are the same as those for the Ni-P-Zr: that is, $Na_2WO_4{\cdot}2H_2O$ (20 g/L) +$NiSO_4$ (30 g/L) + $Na_3C_6H_5O_7{\cdot}2H_2O$ (45 g/L) + NH_4Cl (35 g/L) + $NaPH_2O_2{\cdot}H_2O$ (30 g/L). Fig. 6 (a) presents the XRD patterns of the Ni-P-W films, exhibiting a broad peak indicative of an amorphous structure or poor crystallinity. Additionally, the SAED patterns shown in Figures 6 (b) and 6 (c) display diffuse rings, further confirming the amorphous nature of the Ni-P-W films. Fig. 6 (d) EDS analysis shows 91.09 wt% Ni, 2.06 wt% W, and 6.85 wt% P. The Ni-P-W coating exhibits a friction coefficient of 0.24, a corrosion potential of –0.54 V, a Vickers hardness of 699.5 HV and a fatigue life of 68 times. Ni-P-W alloy-coated films are well-suited for applications requiring exceptional mechanical strength, wear resistance, and thermal stability, making them particularly effective for cutting tools and abrasive environments. However, the Ni-P-Zr alloy-coated films are appropriate for passivation and corrosion protection, especially in marine, biomedical, or oxidative environments. While they exhibit lower hardness than W-based coatings, they offer excellent chemical stability and strong adhesion to substrates.

Fig. 7 shows the SEM images of the surface morphology and cross-section for electroless Ni-P-Zr coatings that are deposited using the orthogonal array electroless parameters (a, b) and the optimal electroless parameters (c, d). The Ni-P-Zr film forms a continuous coating over the substrate, which is characterized by a dense fine-nodular grain structure and no evidence of cracking or delamination and excellent adhesion. The film thickness increases from 1.23 μm ($A_3B_2C_1D_3$) to 2.76 μm ($A_3B_2C_3D_3$).

Electroless plating time affects the thickness, hardness, microstructure, surface morphology and mechanical performance of film coatings [32]. A longer electroless plating time produces a thicker film, finer nodular grains and greater hardness, so the coating is more resistant to wear. These results are in agreement with those of Kao JY [33]. Table 9 lists the experimental results for the fatigue life of Ni-P-Zr coated specimens that use different electroless plating times. The uncoated Al 6061-T6 substrates have a fatigue life of 29 times (high-strain and low-cycle bending fatigue [23]). For substrates with a a Ni-P-Zr coating, the fatigue life increases from 36 to 52 times. Fatigue damage begins with microcracks on the surface of the material, which then expand and develop, and create a fracture. Improving the mechanical properties of the material surface prevents fatigue damage [34].

Figures 8 and 9 compare the failure mechanisms for the original Al substrates to those that are treated using optimal electroless Ni-P-Zr plating parameter values for high-strain, low-cycle fatigue loading. Fig. 8 shows that after bending 10 and 20 times, no obvious microcracks appear on the surface of the specimen, but larger cracks appear at the 25th bending and fatigue fracture occurs at the 29th bending. Fig. 9 shows that for the Ni-P-Zr coated specimens, no significant surface changes are observed after 10 to 40 bending cycles. Microcracks first appear at the 48th bend, followed by larger cracks at the 49th bend, and fatigue fracture occurs at the 52nd bend. The uncoated specimen experiences a fatigue fracture at the 29th bend. These results show that the coating delays crack initiation and propagation and extends the fatigue life of the specimens.

Table 5. *Grey relational grades and their corresponding ranking in the optimization process*

No.	Factors				Grey relational grade	Order
	A	B	C	D		
1	1	1	1	1	0.3647	7
2	1	2	2	2	0.3256	9
3	1	3	3	3	0.4393	5
4	2	1	2	3	0.3569	8
5	2	2	3	1	0.4481	4
6	2	3	1	2	0.3967	6
7	3	1	3	2	0.5827	3
8	3	2	1	3	0.7333	1
9	3	3	2	1	0.6058	2

Table 6. *Grey relational analysis and ANOVA results for evaluating multiple quality properties*

Factor	S/N ratio (dB)			Degree of freedom	Sum of square	Variance	Contribution (P %)
	Level 1	Level 2	Level 3				
A	-8.55	-7.98	-3.91	2	38.40	19.20	83.31
B	-7.47	-6.47	-6.51	2	1.91	0.96	4.15
C	-6.50	-7.68	-6.27	2	3.46	1.73	7.50
D	-6.70	-7.49	-6.26	2	2.32	1.16	5.04
Total				8	42.41		100

Table 7. *Verification experimental results for multiple quality properties using orthogonal arrays and optimal predicted Ni-P-Zr films deposition parameter values*

	Orthogonal array $A_3B_2C_1D_3$	Optimal prediction design $A_3B_2C_3D_3$	Improvement rate
Friction coefficient	0.37	0.35	5.41
Corrosion potential (V)	-0.66	-0.60	9.09
Hardness (HV)	541.5	582.9	7.66

Table 8. *Chemical composition of the Ni-P-Zr films, as measured by energy-dispersive spectrometry (EDS)*

No.	Factors				wt.%			Total
	A	B	C	D	Ni	Zr	P	(%)
1	1	1	1	1	91.33	2.10	6.57	100
2	1	2	2	2	90.69	2.51	6.80	100
3	1	3	3	3	94.19	2.24	3.57	100
4	2	1	2	3	92.00	1.22	6.78	100
5	2	2	3	1	94.30	1.96	3.74	100
6	2	3	1	2	93.76	1.74	4.50	100
7	3	1	2	2	92.49	3.73	3.78	100
8	3	2	1	3	95.72	1.65	2.63	100
9	3	3	3	1	93.57	1.33	5.10	100
Optimal	3	2	3	3	96.02	1.37	2.61	100

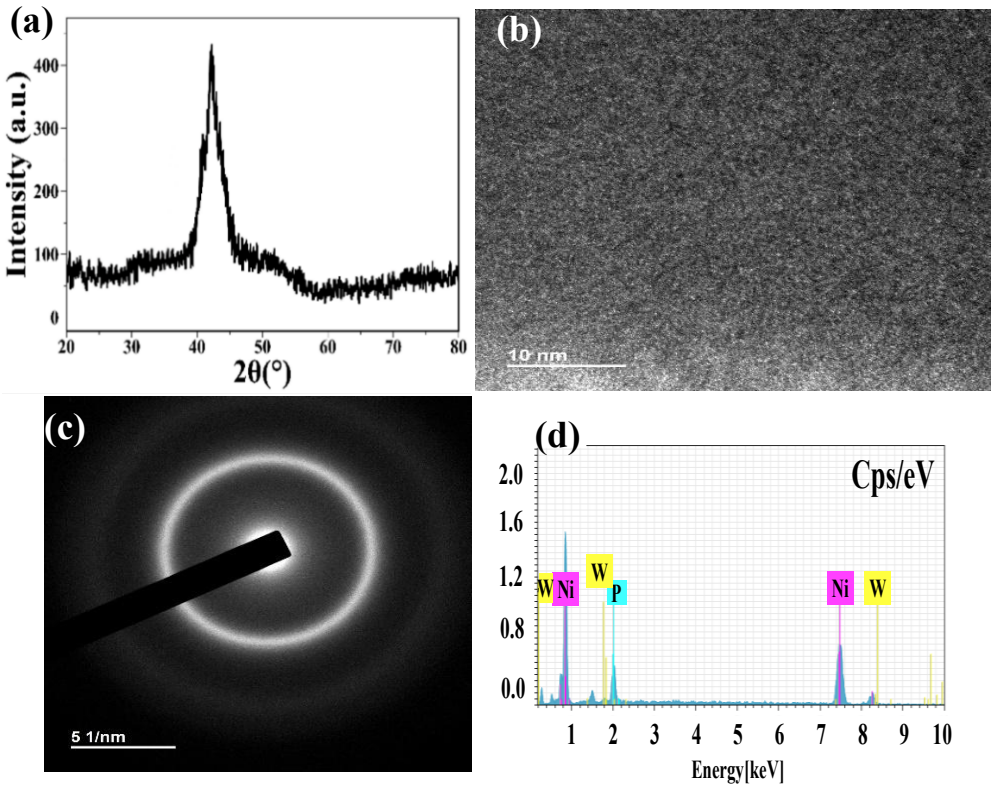

Fig. 6. Electroless N-P-W film: (a) X-ray diffraction pattern, (b) high-resolution TEM image, (c) electronic diffraction pattern, and (b) EDS analysis

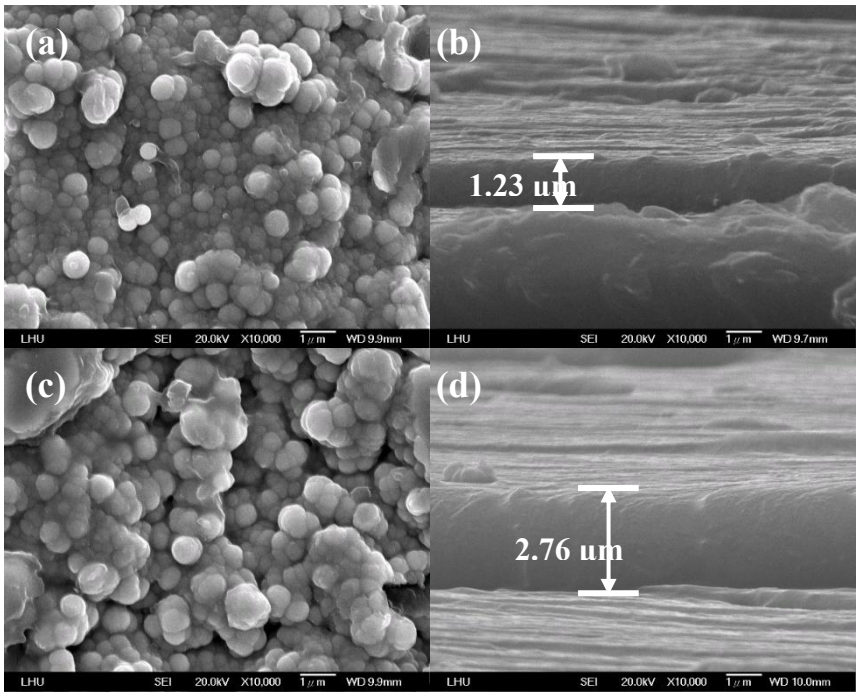

Fig. 7. SEM surface and cross-sectional images of Ni-P-Zr films: (a, b) deposited using orthogonal array parameter values ($A_3B_2C_1D_3$) and (c, d) deposited using optimal prediction design ($A_3B_2C_3D_3$)

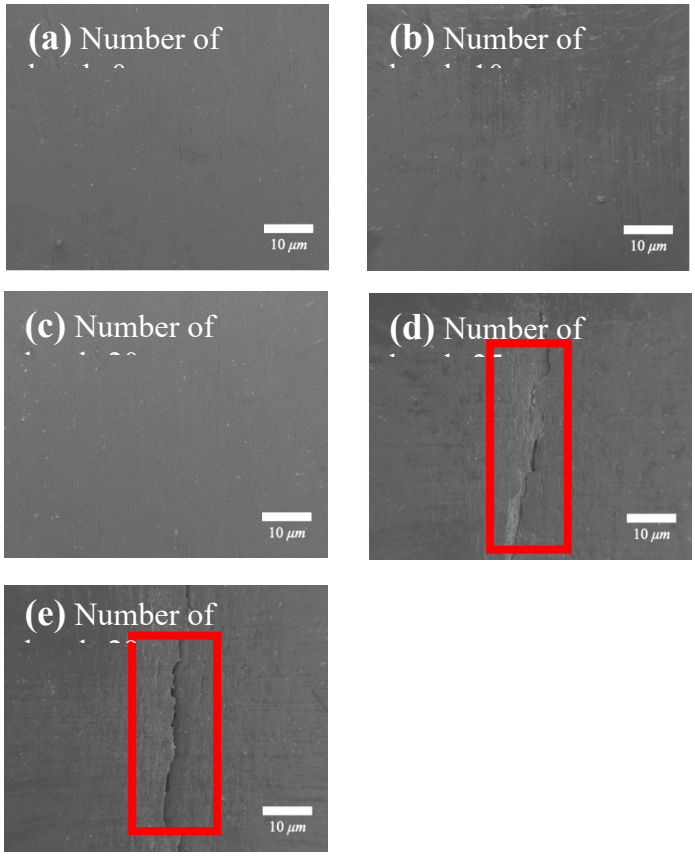

Fig. 8. Failure mechanism for bare Al 6061-T6 substrates for high-strain and low-cycle fatigue testing

Table 9. *Experimental results for the fatigue life of Ni-P-Zr coatings*

No.	Factors				Fatigue life times		Ave.
	A	B	C	D	T_1	T_2	
1	1	1	1	1	38	42	40
2	1	2	2	2	41	40	40
3	1	3	3	3	44	42	43
4	2	1	2	3	41	33	37
5	2	2	3	1	42	40	41
6	2	3	1	2	36	36	36
7	3	1	3	2	45	49	47
8	3	2	1	3	47	51	49
9	3	3	2	1	43	45	44
Optimal	3	2	3	3	53	52	52
Al 6061-T6					29	30	29

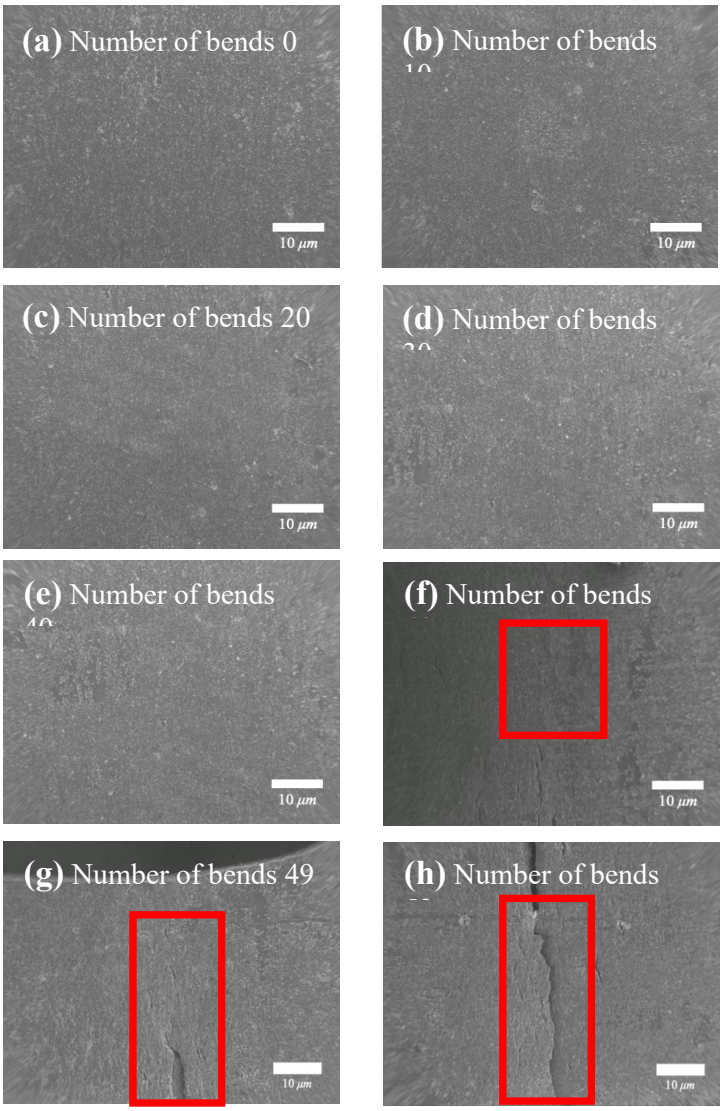

Fig. 9. Failure mechanism for Ni-P-Zr film that is coated using optimal prediction design electroless plating for high-strain and low-cycle fatigue testing

CONCLUSIONS

During the pretreatment of the Al alloy substrates, phosphate and carbonate act as complexing agents and buffering salts, the surface is activated, and a thin zinc-based activation layer is deposited to enhance the adhesion of subsequent electroless coatings and produce a high-quality electroless plating film. Using grey-Taguchi analysis, this study experimentally determines the mechanical properties of electroless Ni-P-Zr coatings and verifies the optimization of parameter values. The results for XRD and TEM analysis show that the as-deposited N-P-Zr film has an amorphous structure. An ANOVA for multiple quality characteristics of the electroless plating process shows that the pH value is the factor that most significantly affects the performance of the electroless N-P-Zr composite film process, contributing 83.31% to the overall performance. Confirmation test results demonstrate the effectiveness of the proposed approach and show an improvement of 5.41% for the coefficient of friction, 9.09% for corrosion potential, and 7.66% for hardness.

The Ni-P-Zr-coated specimens exhibit no significant surface changes after 10 to 40 bending cycles. Microcracks first appear at the 48th bend, and fatigue fracture occurs at the 52nd bend. The uncoated specimen demonstrates a fatigue fracture at the 29th bend. These results show that the coating delays crack initiation and propagation and extends the fatigue life of the specimens. Further, Ni-P-W coatings exhibit superior mechanical properties compared to Ni-P-Zr coated substrates.

ACKNOWLEDGEMENTS

The authors gratefully acknowledge the support of the National Science and Technology Council, Taiwan (ROC) through Grant Nos. NSTC 114-2622-E-262-003. We gratefully thank Ms. Chia-Ying Chien and Su-Jen Ji for the assistance in TEM and FIB experiments of the Instrumentation Center at NTU which is supported by the National Science and Technology Council, Taiwan.

REFERENCES

1. Ahmadian, H., Zhou, T., Guo, W., Yu, Q.: Achieving enhanced electroless Ni–P plating on 6H-SiC substrate through optimization of plasma activation durations. *Surface and Coatings Technology* 495 (2025), 131563. https://doi.org/10.1016/j.surfcoat.2024.131563
2. Kumar, M., Sidpara, A., Racherla, V.: Improving surface finish and wear resistance of electroless nickel plating using flexible abrasive tool. *Wear* 546–547 (2024), 205326. https://doi.org/10.1016/j.wear.2024.205326
3. Biswas, A., Das, S.K., Sahoo, P.: Correlating tribological performance with phase transformation behavior for electroless Ni-(high) P coating. *Surface and Coatings Technology* 328 (2017), 102–114. https://doi.org/10.1016/j.surfcoat.2017.08.043
4. Yildiz, R.A., Genel, K., Gulmez, T.: Effect of electroless Ni–B and Ni–W–B coatings on the corrosion–fatigue behaviour of 7075 Al alloy. *International Journal of Fatigue* 144 (2021), 106040. https://doi.org/10.1016/j.ijfatigue.2020.106040
5. Arumugam, A., Lakshmanan, P., Palani, S., Parthiban, K.: Wear behavior of Ni–P and Al_2O_3 electroless nano coating on aluminium alloy. *Materials Today: Proceedings* 46 (2021), 1066–1070.

https://doi.org/10.1016/j.matpr.2021.01.425

6. Qin, W.: Microstructure and corrosion behavior of electroless Ni–P coatings on 6061 aluminum alloys. *Journal of Coatings Technology and Research* 8 (2011), 135–139. https://doi.org/10.1007/s11998-010-9256-3
7. Mohamed Anuar, R.A., Ismail, A., Ismail, N., Taib, I., Abd Latif, N.S., Hamdan, I.F., A Razak, S.A.: Optimisation of electroless nickel electroless palladium immersion silver (ENEPImAg) surface finish parameters using the Taguchi method for enhanced solder joint reliability. *Soldering & Surface Mount Technology* 37(4) (2025), 279–295. https://doi.org/10.1108/SSMT-10-2024-0059
8. Agrawal, R., Prakash, O., Brar, L.S., Mukhopadhyay, A.: A systematic investigation of lead-free electroless Ni–B–W coating properties using Taguchi's methodology. *Coatings* 13 (2023), 1585. https://doi.org/10.3390/coatings13091585
9. Kumar, S., Ghosh, S.K., Pawar, N.N., Rathod, S.H., Chaudhari, M.A., Bhagat, R.R., Goli, R.: Design of experiment with tribological performance analysis of electroless nano-composite Ni–P–SiC coating for conveyors. *Tribology in Industry* 44 (2022), 707–718. https://doi.org/10.24874/ti.1371.09.22.11
10. Gultekin, D., Duru, E., Uysal, M., Akbulut, H.: Tribological and corrosive properties examination of graphene oxide enriched electroless Ni–P–W composite coatings. *Surface and Coatings Technology* 488 (2024), 131084. https://doi.org/10.1016/j.surfcoat.2024.131084
11. Biswas, A., Das, S.K., Sahoo, P.: Effect of copper incorporation on phase transformation behavior of electroless nickel–phosphorous coating and its effect on the tribological behavior. *Proceedings of the Institution of Mechanical Engineers, Part L: Journal of Materials: Design and Applications* 235 (2021), 898–916. https://doi.org/10.1177/1464420720981602
12. Sharma, T., Bera, H., Brown, D.A., Schulze, A., Bruening, R.: Thermal evolution, phase composition and fracture toughness of electroless Ni–P, Ni–W–P and Ni–Mo–W–P films for solderable surfaces on copper. *Surface and Coatings Technology* 467 (2023), 129722. https://doi.org/10.1016/j.surfcoat.2023.129722
13. Lu, H.J., Wu, H., Zou, N., Lu, X.G., He, Y.L., Morgan, D.: First-principles investigation on diffusion mechanism of alloying elements in dilute Zr alloys. *Acta Materialia* 154 (2018), 161–171. https://doi.org/10.1016/j.actamat.2018.05.015
14. Agarwala, R.C., Sharma, R.: Electroless Ni–P nano coating technology. *Synthesis and Reactivity in Inorganic, Metal-Organic and Nano-Metal Chemistry* 38 (2008), 229–236. https://doi.org/10.1080/15533170801926598
15. Zhao, Y.C., Chen, D.Y., Hu, D.C., Li, J.R., Hsu, C.Y.: Application of Taguchi grey analysis to optimization of mechanical properties of ZrWN/buffer multilayer coatings. *International Journal of Electrochemical Science* 14 (2019), 4520–4531. https://doi.org/10.20964/2019.05.22
16. Ganesan, K., Selvan, D.K., Madhu, M., Archana, G.: Mechanical behaviour and low cycle fatigue performance of plasma sprayed ZrO_2 coated Al-7075-T6 alloy under subzero temperature condition. *Journal of Alloys and Compounds* 1016 (2025), 178950. https://doi.org/10.1016/j.jallcom.2025.178950
17. Li, P.W., Hsu, C.W., Yan, C.S., Hsu, C.Y., Hung, C.H., Kao, J.Y.: Structure and fatigue behavior of electroless plated Ni–Zn–P films using pretreatments, annealing and an applied magnetic field. *International Journal of Fatigue* 167 (2023), 107369. https://doi.org/10.1016/j.ijfatigue.2022.107369
18. Zhou, J.Z., Huang, S., Sheng, J., Lu, J.Z., Wang, C.D., Chen, K.M., Ruan, H.Y., Chen, H.S.: Effect

of repeated impacts on mechanical properties and fatigue fracture morphologies of 6061-T6 aluminum subject to laser peening. *Materials Science and Engineering A* 539 (2012), 360–368. https://doi.org/10.1016/j.msea.2012.01.125

19. Kocabas, M., Ornek, C., Curioni, M., Cansever, N.: Nickel fluoride as a surface activation agent for electroless nickel coating of anodized AA1050 aluminum alloy. *Surface and Coatings Technology* 364 (2019), 231–238. https://doi.org/10.1016/j.surfcoat.2019.03.003
20. Mandal, R., Mondal, N., Ghosh, A., Mallick, A., Sarkar, S., Mandal, T., Sen, R.S., Majumdar, G.: Estimation of surface roughness upon electroless Ni–Fe–P coatings: experiments, characterization, modelling and optimization. *International Journal on Interactive Design and Manufacturing* 19 (2025), 1–15. https://doi.org/10.1007/s12008-025-02270-1
21. Li, X., Chen, C.S., Tsao, C.C., Hu, C.C., Chen, C., Hsu, C.Y.: Characteristics of DLC films doped with multi-element alloy. *The International Journal of Advanced Manufacturing Technology* 121 (2022), 2631–2646. https://doi.org/10.1007/s00170-022-09519-z
22. Zhuang, Q., Lin, N., He, Y., Kang, X.: Influence of temperature on sintering behavior and properties of TiC–Fe–Co–Ni–Cr–Mo cermets. *Ceramics International* 43 (2017), 15992–15998. https://doi.org/10.1016/j.ceramint.2017.08.186
23. Kuo, C.G., Hsu, C.Y., Chen, J.H., Lee, P.W.: Discharge current effect on machining characteristics and mechanical properties of aluminum alloy 6061 workpiece produced by electric discharging machining process. *Advances in Mechanical Engineering* 9 (2017), 1–8. https://doi.org/10.1177/1687814017730756
24. Liu, Z., Liu, Z., Wang, D., Wang, B., Ding, F., Wang, L., Chen, Y., Yang, Y., Wang, B.: Surface state study of the pre-treatment process for electroless plated aluminum alloys for EP mandrels. *Radiation Detection Technology and Methods* (2025), 1–12. https://doi.org/10.1007/s41605-024-00516-2
25. Makoto, H.I.N.O., Murakami, K., Mitooka, Y., Muraoka, K., Kanadani, T.: Effects of zincate treatment on adhesion of electroless Ni–P coating onto various aluminum alloys. *Transactions of Nonferrous Metals Society of China* 19 (2009), 814–818. https://doi.org/10.1016/S1003-6326(08)60356-8
26. Unni, M., Sudagar, J.: Preparation of electroless deposition of NiTiZr (P) quaternary alloy and their properties. *Heliyon* 10 (2024), e37363. https://doi.org/10.1016/j.heliyon.2024.e37363
27. Niedbała, J., Popczyk, M., Benke, G., Okła, H., Gabor, J., Wrzalik, R., Stanula, A., Swinarew, A.S.: The use of ZrO_2 waste for the electrolytic production of composite Ni–P–ZrO_2 powder. *Materials* 14 (2021), 6597. https://doi.org/10.3390/ma14216597
28. Agrawal, R., Mukhopadhyay, A.: Optimization of wear rate and COF of heat treated electroless Ni–B–W coating from a stabilizer free bath using grey relational analysis. *Materials Today: Proceedings* 91 (2023), 119–124. https://doi.org/10.1016/j.matpr.2023.05.653
29. Ghaderi, M., Rezagholizadeh, M., Monir Vaghefi, S.M., Heidary, A.: Investigation of high temperature wear resistance of electroless nickel coating with different contents of phosphorous. *Protection of Metals and Physical Chemistry of Surfaces* 52 (2016), 538–542. https://doi.org/10.1134/S2070205116030126
30. Agarwala, R.C., Agarwala, V.: Electroless alloy/composite coatings: A review. *Sadhana* 28 (2003), 475–493. https://doi.org/10.1007/BF02706445
31. Rajendran, R., Sha, W., Elansezhian, R.: Abrasive wear resistance of electroless Ni–P coated aluminium after post treatment. *Surface and Coatings Technology* 205 (2010), 766–772. https://doi.org/10.1016/j.surfcoat.2010.07.124

32. Ashassi-Sorkhabi, H., Rafizadeh, S.H.: Effect of coating time and heat treatment on structures and corrosion characteristics of electroless Ni–P alloy deposits. *Surface and Coatings Technology* 176 (2004), 318–326. https://doi.org/10.1016/S0257-8972(03)00746-1

33. Kao, J.Y.: Improvement in the working life of a micro journal bearings with an electroless Ni–P coating. The International Journal of Advanced Manufacturing Technology 119 (2022), 7487–7502. https://doi.org/10.1007/s00170-022-08699-y

34. Szusta, J., Seweryn, A.: Low-cycle fatigue model of damage accumulation–The strain approach. *Engineering Fracture Mechanics* 77 (2010), 1604–1616. https://doi.org/10.1016/j.engfracmech.2010.04.014